

Quantum-enhanced interferometry with unbalanced entangled coherent states

Jun Tang(汤俊), Zi-Hang Du(堵子航), Wei Zhong(钟伟), Lan Zhou(周澜), and Yu-Bo Sheng(盛宇波)

Citation: Chin. Phys. B, 2025, 34 (**2**): 020303. DOI: 10.1088/1674-1056/ad99ca
Journal homepage: http://cpb.iphy.ac.cn; http://iopscience.iop.org/cpb

What follows is a list of articles you may be interested in

Parameter estimation in *n*-dimensional massless scalar field

Ying Yang(杨颖) and Jiliang Jing(荆继良)
Chin. Phys. B, 2024, 33 (**3**): 030307. DOI: 10.1088/1674-1056/ad1749

Holevo bound independent of weight matrices for estimating two parameters of a qubit

Chang Niu(牛畅) and Sixia Yu(郁司夏)
Chin. Phys. B, 2024, 33 (**2**): 020304. DOI: 10.1088/1674-1056/ad117d

Quantum interferometric power and non-Markovianity in the decoherence channels

Shaojie Xiong(熊少杰), Zhe Sun(孙哲), and Xiaoguang Wang(王晓光)
Chin. Phys. B, 2023, 32 (**8**): 080302. DOI: 10.1088/1674-1056/accb4e

Improving the teleportation of quantum Fisher information under non-Markovian environment

Yan-Ling Li(李艳玲), Yi-Bo Zeng(曾艺博), Lin Yao(姚林), and Xing Xiao(肖兴)
Chin. Phys. B, 2023, 32 (**1**): 010303. DOI: 10.1088/1674-1056/ac6497

Hybrid entanglement concentration assisted with single coherent state

Rui Guo(郭锐), Lan Zhou(周澜), Shi-Pu Gu(顾世浦),Xing-Fu Wang(王兴福), Yu-Bo Sheng(盛宇波)
Chin. Phys. B, 2016, 25 (**3**): 030302. DOI: 10.1088/1674-1056/25/3/030302

SPECIAL TOPIC — Quantum communication and quantum network

Quantum-enhanced interferometry with unbalanced entangled coherent states

Jun Tang(汤俊)[1], Zi-Hang Du(堵子航)[1], Wei Zhong(钟伟)[1,†]
Lan Zhou(周澜)[2], and Yu-Bo Sheng(盛宇波)[3]

[1] *Institute of Quantum Information and Technology, Nanjing University of Posts and Telecommunications, Nanjing* 210003, *China*
[2] *School of Science, Nanjing University of Posts and Telecommunications, Nanjing* 210003, *China*
[3] *College of Electronic and Optical Engineering and College of Flexible Electronics (Future Technology), Nanjing University of Posts and Telecommunications, Nanjing* 210003, *China*

(Received 11 September 2024; revised manuscript received 13 November 2024; accepted manuscript online 3 December 2024)

We propose a quantum-enhanced metrological scheme utilizing unbalanced entangled coherent states (ECSs) generated by passing a coherent state and a coherent state superposition through an unbalanced beam splitter (BS). We identify the optimal phase sensitivity of this scheme by maximizing the quantum Fisher information (QFI) with respect to the BS transmission ratio. Our scheme outperforms the conventional scheme with a balanced BS, particularly in the presence of single-mode photon loss. Notably, our scheme retains quantum advantage in phase sensitivity in the limit of high photon intensity, where the balanced scheme offers no advantage over the classical strategy.

Keywords: quantum-enhanced interferometry, entangled coherent state, quantum Fisher information

PACS: 03.65.Ta, 42.50.–p, 42.50.St, 42.79.–e

DOI: 10.1088/1674-1056/ad99ca **CSTR:** 32038.14.CPB.ad99ca

1. Introduction

Optical interferometers[1–5] are among the most precise measurement instruments and are widely used in applications such as gravitational waves[6,7] and imaging.[8,9] These devices transform the task of measuring an unknown physical quantity of interest into inferring the relative phase shift between the two optical modes propagating along different arms of the interferometer. Consequently, the sensitivity of phase estimation becomes a critical factor in determining the effectiveness of precision measurements. In classical linear phase estimation, the ultimate phase sensitivity is limited by the shot-noise limit,[2,10,11] $1/\sqrt{N}$, where N represents the mean photon number of the input state. This can be bettered when employing non-classical probes, such as NOON states,[1,12,13] squeezed states,[14–18] Fock states[19,20] and entangled coherent states (ECSs).[21–23]

Among these states, NOON states can achieve a Heisenberg scaling limit in sensitivity, offering a $\sqrt{N}$ factor improvement over the shot-noise limit. However, in practice, NOON states are fragile and highly susceptible to deterioration from photon loss,[13] ultimately losing their quantum advantage in sensitivity enhancement. In Ref. [21], Joo *et al.* proposed a more robust quantum-enhanced scheme by using balanced ECSs as probe states. A balanced ECS is generated by injecting a coherent state and a coherent state superposition into a balanced beam splitter (BS). The balanced ECS was initially proposed by A. Luis for lossless phase estimation.[24] Joo *et al.* demonstrated the ultimate phase sensitivity under photon loss by numerically calculating the quantum Fisher information (QFI). Their findings showed that balanced ECSs not only achieve better sensitivity than NOON states but are also more resilient to photon loss.[21] Analytical approaches to this issue were subsequently developed.[25,26] However, these works were limited to the balanced BS configuration, which is commonly used in conventional optical interferometers.[21,25,26]

In this paper, we extend the balanced configuration to an unbalanced one, inspired by recent studies on interferometers with unbalanced BSs.[27–30] We also utilize a coherent state and a coherent state superposition as input states. The resulting state after passing through an unbalanced BS is referred to as an unbalanced ECS. We analyze the phase sensitivity of these states using QFI theory and identify the optimal phase sensitivity with respect to the transmittance of the BS for both single- and two-mode photon loss scenarios. We elucidate that the unbalanced configuration is superior to the balanced one in phase estimation under conditions of photon loss, in contrast to the results obtained with the balanced scheme.[21,25,26] Moreover, we clarify that the sensitivity enhancement advantage of the balanced configuration holds only when the photon intensity is low under both single- and double-mode photon loss. However, this advantage diminishes as the photon number increases, finally becoming equivalent to the sensitivity achieved

[†]Corresponding author. E-mail: zhongwei1118@gmail.com

© 2025 Chinese Physical Society and IOP Publishing Ltd. All rights, including for text and data mining, AI training, and similar technologies, are reserved.

with a coherent state. In contrast, our unbalanced configuration exhibits more robust performance regardless of photon intensity for the single-mode photon loss case.

This paper is organized as follows. In Section 2, we provide a brief introduction to QFI theory and derive the exact expression of the QFI for two-mode states. In Section 3, we propose a quantum enhanced interferometry scheme and discuss the optimal phase sensitivity of this scheme in the presence of photon losses. In Section 4, we compare the performance of balanced and unbalanced ECSs in phase estimation when the photon intensity is high. Finally, our conclusion is provided in Section 5.

2. Quantum Fisher information formalism for two-mode states

Consider a parametric density matrix $\tilde{\rho}_\phi$ that depends on an unknown parameter ϕ, which we aim to estimate. According to the quantum estimation theory, the ultimate sensitivity for estimating ϕ is governed by the quantum Cramér–Rao bound as

$$(\delta\hat{\phi})^2 \geq \frac{1}{mF}, \tag{1}$$

where $\hat{\phi}$ is the estimator of the parameter, m represents the number of repetitions of the experiment and F denotes the so-called QFI.[31–33] This bound represents the best achievable sensitivity with optimal detection. Given the optimal detection, the bound of Eq. (1) can be reached by the maximum likelihood estimator in the asymptotic limit of large m. From Eq. (1), the estimation sensitivity is limited by the inverse of the QFI, which suggests that the larger the value of the QFI the higher the possible sensitivity of phase estimation.

Choosing a measurement that saturates the ultimate sensitivity is crucial for the practical implementation of quantum metrological schemes. According to quantum parameter estimation theory, the symmetric logarithmic derivative (SLD) operator represents the optimal measurement observable for saturating the quantum Cramér–Rao bound.[33–35] However, implementing the SLD measurement in realistic experiments poses challenges, as it often depends on the phase parameter to be estimated, making it potentially unfeasible. Recent advances have been made in simulating arbitrary measurements using post-selection,[36] quantum walks[37] or adaptive schemes.[38] Therefore, in our work, we assume that SLD measurement is feasible and focus on identifying the ultimate sensitivity achievable with unbalanced ECSs.

We assume that the parametric density matrix $\tilde{\rho}_\phi$ is generated by applying a ϕ-dependent unitary evolution[39–41]

$$U = \exp(-\mathrm{i}\phi G) \tag{2}$$

to the initial state $\tilde{\rho}$, where G is the Hermitian generator associated with the parameter ϕ. Below, we provide the exact expression for the QFI for an arbitrary two-mode state. For simplicity, we first consider a two-dimensional density matrix $\tilde{\rho}$, the spectral decomposition of which is given by

$$\tilde{\rho} = p_1 |\varphi_1\rangle\langle\varphi_1| + p_2 |\varphi_2\rangle\langle\varphi_2|, \tag{3}$$

with the condition $p_1 + p_2 = 1$. In this decomposition, the two basis states $|\varphi_1\rangle$ and $|\varphi_2\rangle$ are assumed to be orthogonal. The QFI for this two-dimensional case can be expressed as[33,42]

$$F = 4\left(p_1\Delta^2 G_1 + p_2\Delta^2 G_2 - 4p_1p_2|G_{12}|^2\right), \tag{4}$$

where

$$\Delta^2 G_i = \langle\varphi_i| G^2 |\varphi_i\rangle - \langle\varphi_i| G |\varphi_i\rangle^2 \tag{5}$$

is the variance of the generator G in the state $|\varphi_i\rangle$, and

$$G_{12} = \langle\varphi_1| G |\varphi_2\rangle \tag{6}$$

is the off-diagonal matrix element of the generator G between the states $|\varphi_1\rangle$ and $|\varphi_2\rangle$.

Next, we extend the formalism for calculating the QFI to the case of a density matrix based on a non-orthogonal basis. This approach was first introduced by Jing *et al.*,[25] and it will be adopted in our subsequent analysis. Let us briefly review it here (see Appendix A for details). Consider an arbitrary 2×2 density matrix expressed as

$$\rho = \begin{pmatrix} a & b \\ b^* & c \end{pmatrix} \tag{7}$$

based on the non-orthogonal normalized basis $|\Psi_1\rangle$ and $|\Psi_2\rangle$. By performing the spectral decomposition of ρ as

$$\rho = \lambda_+ |\lambda_+\rangle\langle\lambda_+| + \lambda_- |\lambda_-\rangle\langle\lambda_-| \tag{8}$$

in a well-defined orthogonal basis $|\lambda_\pm\rangle = \mathcal{C}_\pm |\Psi_1\rangle + \mathcal{D}_\mp |\Psi_2\rangle$, associated with the eigenvalues $\lambda_\pm$ (see Appendix A for explicit definitions), and according to Eq. (4), the QFI for the state given by Eq. (7) can be represented as

$$F = 4\left(\lambda_+\Delta^2 G_+ + \lambda_-\Delta^2 G_- - 4\lambda_+\lambda_- |G_{+-}|^2\right), \tag{9}$$

where

$$\Delta^2 G_\pm = \langle\lambda_\pm| G^2 |\lambda_\pm\rangle - \langle\lambda_\pm| G |\lambda_\pm\rangle^2, \tag{10}$$

$$G_{+-} = \langle\lambda_+| G |\lambda_-\rangle. \tag{11}$$

3. Quantum optical interferometry with unbalanced ECSs

A standard Mach–Zehnder interferometer (MZI) generally consists of two BSs denoted by B and a phase shifter denoted by U (see Fig. 1). This configuration illustrates the principle of phase estimation. The input light is split into two

modes by the first BS. The signal mode marked by 1 accumulates an unknown phase ϕ through the phase-shifting operation, as discussed in Refs. [21,25,26]. The phase operation can be described by

$$U = \exp\left(-\mathrm{i}\phi a_1^\dagger a_1\right), \tag{12}$$

with a_1 and $a_1^\dagger$ representing the annihilation and creation operators for the signal mode 1, respectively. The phase is then determined by detecting the photons exiting from the second BS.

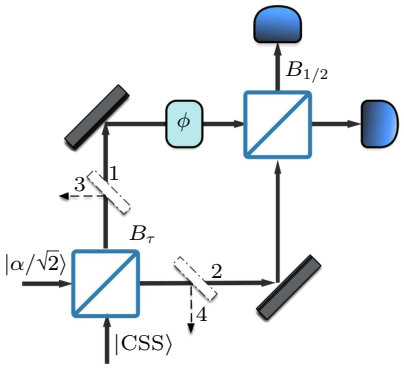


Fig. 1. Schematic of a Mach–Zehnder interferometer with an unbalanced BS of variable transmittance τ fed by a coherent state $|\alpha/\sqrt{2}\rangle$ and a coherent state superposition $|\mathrm{CSS}\rangle$.

In a typical MZI, the BSs are often assumed to be balanced, with a 50 : 50 ratio of reflectivity to transmittance. Under these conditions, Joo *et al.* proposed a balanced ECS scheme for phase estimation.[21] Their scheme involves injecting a coherent state and a coherent state superposition into the input ports of the first BS. The output from this balanced BS generates the so-called balanced ECS, which has been demonstrated to be superior to the NOON state scheme in scenarios with photon losses.[21,25,26]

Here, we propose a modified ECS scheme that utilizes an unbalanced BS instead of a balanced one. Such an unbalanced configuration has been shown to provide advantages for phase estimation tasks.[27,29,34] In our scheme, an unbalanced BS is represented by

$$B_\tau = \exp\left[\arccos\sqrt{\tau}\left(a_1 a_2^\dagger - a_1^\dagger a_2\right)\right], \tag{13}$$

where τ denotes the variable transmittance of the BS and a_2 and $a_2^\dagger$ represent the annihilation and creation operators for the idler mode 2, respectively. Unlike Joo *et al.*'s scheme, the coherent state $\left|\alpha/\sqrt{2}\right\rangle$ and the coherent state superposition are input into each port of a variable BS B_τ, respectively, rather than a balanced one. The coherent state superposition is given by

$$|\mathrm{CSS}\rangle = \mathcal{N}\left(\left|\frac{\alpha}{\sqrt{2}}\right\rangle + \left|-\frac{\alpha}{\sqrt{2}}\right\rangle\right), \tag{14}$$

with $\mathcal{N} = 1/\sqrt{2\left(1+\mathrm{e}^{-|\alpha|^2}\right)}$ as the normalization coefficient. After passing through the variable BS, this state evolves into a τ-dependent ECS, expressed as

$$\begin{aligned}|\mathrm{ECS}\rangle_\tau = \mathcal{N}\Bigg(&\left|\frac{\alpha\chi_+}{\sqrt{2}}\right\rangle_1\left|\frac{\alpha\chi_-}{\sqrt{2}}\right\rangle_2 \\ &+\left|-\frac{\alpha\chi_-}{\sqrt{2}}\right\rangle_1\left|\frac{\alpha\chi_+}{\sqrt{2}}\right\rangle_2\Bigg),\end{aligned} \tag{15}$$

with $\chi_\pm = \sqrt{\tau} \pm \sqrt{1-\tau}$. When $\tau = 1/2$, i.e., the balance case, associated with $\chi_+ = \sqrt{2}$ and $\chi_- = 0$, the expression of Eq. (15) simplifies to

$$|\mathrm{ECS}\rangle = \mathcal{N}\left(|\alpha\rangle_1|0\rangle_2 + |0\rangle_1|\alpha\rangle_2\right). \tag{16}$$

This state is known as the balanced ECS.[21,25,26]

3.1. Photon loss in a single arm

3.1.1. Photon loss in signal mode

In the following, we use the unbalanced ECS given by Eq. (15) as the probe state for phase estimation in a lossy interferometer. We first consider the scenario where photon loss occurs in the signal mode of the interferometer. This assumption represents an extreme case where photon loss in the signal mode is more significant than in the idler mode.[44] Photon loss is typically modeled by inserting a virtual BS of the reflectivity η into the interferometer mode, denoted as V.[45] After undergoing photon loss, the signal mode accumulates an unknown phase parameter ϕ through the operation defined in Eq. (12). While photon loss can occur throughout the entire phase-shifting process, the commutation relationship between phase shifting and photon loss[39,40] allows the order of these operations to be interchanged. For simplicity, we assume that photon loss occurs before phase shifting.

After undergoing photon loss in the signal mode, the unbalanced ECS from Eq. (15) evolves into a mixed state, which can be expressed as

$$\begin{aligned}\rho_{1,2}^{\mathrm{S}} &= \mathrm{Tr}_3\left[V_{1,3}\left(|\mathrm{ECS}\rangle_\tau\langle\mathrm{ECS}|\otimes|0\rangle_3\langle 0|\right)V_{1,3}^\dagger\right] \\ &= \mathcal{N}^2\Bigg[\left|\frac{\beta\chi_+}{\sqrt{2}}\right\rangle_1\left\langle\frac{\beta\chi_+}{\sqrt{2}}\right|\otimes\left|\frac{\alpha\chi_-}{\sqrt{2}}\right\rangle_2\left\langle\frac{\alpha\chi_-}{\sqrt{2}}\right| \\ &\quad+\left|-\frac{\beta\chi_-}{\sqrt{2}}\right\rangle_1\left\langle-\frac{\beta\chi_-}{\sqrt{2}}\right|\otimes\left|\frac{\alpha\chi_+}{\sqrt{2}}\right\rangle_2\left\langle\frac{\alpha\chi_+}{\sqrt{2}}\right| \\ &\quad+\mathrm{e}^{-\tau\eta|\alpha|^2}\left|\frac{\beta\chi_+}{\sqrt{2}}\right\rangle_1\left\langle-\frac{\beta\chi_-}{\sqrt{2}}\right|\otimes\left|\frac{\alpha\chi_-}{\sqrt{2}}\right\rangle_2\left\langle\frac{\alpha\chi_+}{\sqrt{2}}\right| \\ &\quad+\mathrm{e}^{-\tau\eta|\alpha|^2}\left|-\frac{\beta\chi_-}{\sqrt{2}}\right\rangle_1\left\langle\frac{\beta\chi_+}{\sqrt{2}}\right|\otimes\left|\frac{\alpha\chi_+}{\sqrt{2}}\right\rangle_2\left\langle\frac{\alpha\chi_-}{\sqrt{2}}\right|\Bigg],\end{aligned} \tag{17}$$

where $\beta \equiv \alpha\sqrt{1-\eta}$ represents the attenuated amplitude of α and the environment corresponding to mode 3 is assumed to

be in a vacuum state. We define

$$|\Psi_1^{\rm S}\rangle = \left|\frac{\beta\chi_+}{\sqrt{2}}\right\rangle_1 \left|\frac{\alpha\chi_-}{\sqrt{2}}\right\rangle_2,$$
$$|\Psi_2^{\rm S}\rangle = \left|-\frac{\beta\chi_-}{\sqrt{2}}\right\rangle_1 \left|\frac{\alpha\chi_+}{\sqrt{2}}\right\rangle_2. \tag{18}$$

Note that the amplitude in mode 1 depends on β, while the amplitude in mode 2 depends on α, since photon loss occurs only in mode 1. In this non-orthogonal basis, the expression for Eq. (17) can be rewritten as

$$\rho_{1,2}^{\rm S} = \mathcal{N}^2 \begin{pmatrix} 1 & {\rm e}^{-\tau\eta|\alpha|^2} \\ {\rm e}^{-\tau\eta|\alpha|^2} & 1 \end{pmatrix}. \tag{19}$$

It is important to note that the off-orthogonal element depends on the BS transmittance τ, which plays a significant role and can lead to substantial differences between the unbalanced and balanced schemes, especially when α is sufficiently large (see Section 4 for a detailed discussion).

To compute the QFI for the case considered above, we first derive the necessary terms from Eqs. (A7)–(A9)

$$\det\rho_{1,2}^{\rm S} = \mathcal{N}^4\left(1-|p^2|\right)\left(1-{\rm e}^{-2\tau\eta|\alpha|^2}\right), \tag{20}$$
$$\langle\sigma_3\rangle = 1-2\mathcal{N}^2\left(1-|p|^2\right), \tag{21}$$
$${\rm e}^{{\rm i}\vartheta} = 1, \tag{22}$$

with the overlap between $|\Psi_1^{\rm S}\rangle$ and $|\Psi_2^{\rm S}\rangle$ given by

$$p \equiv \langle\Psi_1^{\rm S}|\Psi_2^{\rm S}\rangle = {\rm e}^{-(1-\tau\eta)|\alpha|^2}. \tag{23}$$

Additionally, we compute the following expectations:

$$\langle\Psi_i^{\rm S}|a_1^\dagger a_1|\Psi_i^{\rm S}\rangle = \frac{\chi_\pm^2}{2}|\alpha|^2(1-\eta), \tag{24}$$
$$\langle\Psi_i^{\rm S}|(a_1^\dagger a_1)^2|\Psi_i^{\rm S}\rangle = \frac{\chi_\pm^2}{2}|\alpha|^2(1-\eta) + \frac{\chi_\pm^4}{4}|\alpha|^4(1-\eta)^2, \tag{25}$$
$$\langle\Psi_1^{\rm S}|a_1^\dagger a_1|\Psi_2^{\rm S}\rangle = \frac{1-2\tau}{2}|\alpha|^2(1-\eta)p, \tag{26}$$
$$\langle\Psi_1^{\rm S}|(a_1^\dagger a_1)^2|\Psi_2^{\rm S}\rangle = \frac{1-2\tau}{2}|\alpha|^2(1-\eta)p + \frac{(1-2\tau)^2}{4}|\alpha|^4(1-\eta)^2 p, \tag{27}$$

where $i=1$ and 2 correspond to $+$ and $-$ in the first two expressions. Substituting these results into Eq. (9) ultimately yields the QFI. However, the expression is cumbersome, so we proceed with numerical calculations to plot the QFI.

In Fig. 2 we plot the QFI as a function of τ for the signal-mode photon loss scenario. From Figs. 3(a) and 3(b), it is clear that the QFI decreases as the photon loss strength increases. In the lossless case ($\eta=0$), the QFI reaches its maximum at $\tau=1/2$, indicating that a balanced BS provides the highest sensitivity for phase estimation. However, when photon loss is present, an unbalanced BS outperforms the balanced one in enhancing phase sensitivity. As photon loss becomes stronger, the optimal BS transmittance $\tau_{\rm opt}$ shifts to smaller values. To understand this behavior, we calculate the average photon number of the signal mode after the first BS

$$\langle a_1^\dagger a_1\rangle = \mathcal{N}^2|\alpha|^2\left[1-(2\tau-1)\,{\rm e}^{-|\alpha|^2}\right]. \tag{28}$$

This calculation shows that decreasing τ increases the average photon number in the signal mode, compensating for the intensity loss due to photon loss and thereby enhancing phase sensitivity compared with the case with $\tau=1/2$.[21,25,26]

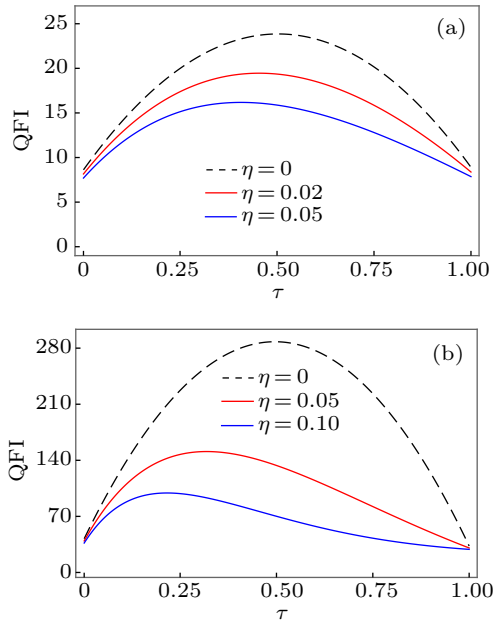


Fig. 2. QFI as a function of the BS transmittance τ for $\alpha=2$ (a) and $\alpha=4$ (b) for different values of η.

In Fig. 3, we plot the QFI as a function of η. For moderate values of η, the unbalanced BS provides greater enhancement in phase sensitivity in comparison with the balanced case.[21,25,26] This enhancement becomes more pronounced as the amplitude α increases. To further highlight the advantage of our scheme, we use the QFI for $\tau=1/2$ as a benchmark[21,25,26] and plot the gain in the QFI for $\tau_{\rm opt}$ relative to $\tau_{1/2}$ in Figs. 3(c) and 3(d). The gain is defined as

$$g_1 = 10\log_{10}\left[\frac{F(\tau_{\rm opt})}{F(\tau_{1/2})}\right]. \tag{29}$$

The plot shows that g depends on η and reaches a maximum of 0.5 dB near the sweet point $\eta=0.46$ for $\alpha=2$ and 2.55 dB near 0.23 for $\alpha=4$, respectively. It is evident that a higher gain is achieved as α increases. Apart from these sweet points, g gradually decreases and becomes zero at $\eta=0$, indicating that the unbalanced BS could still provide enhancement in phase sensitivity over the full range of η, except at $\eta=0$ and $\eta=1$, where the balanced configuration remains optimal,

as shown in Figs. 3(c) and 3(d). As depicted in the insets, the value of the optimal BS transmittance decreases monotonically from 0.5 to nearly 0 as η increases.

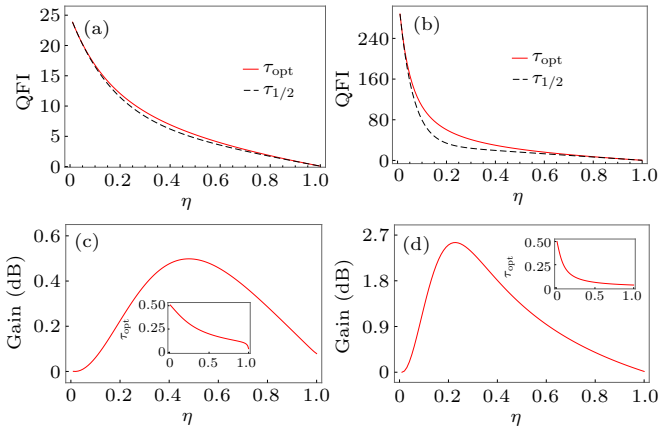


Fig. 3. QFI as a function of the photon loss strength η in the upper panel and the gain defined in Eq. (29) as a function of η in the lower panel. We set $\alpha = 2$ (a), (c) and $\alpha = 4$ (b), (d). In (a) and (b), the red solid line represents the QFI for the BS with the optimal transmittance $\tau_{\rm opt}$, while the black dashed line is for the balanced BS $\tau_{1/2}$. In the inserts, the optimal $\tau_{\rm opt}$ versus η is plotted.

3.1.2. Photon loss in idler mode

In contrast to the previous scenario, we now consider another single-mode photon loss case, where photon loss occurs only in the idler mode of the interferometer. Following the procedure described in Subsection 3.1.1, the density matrix of the system after photon loss can be expressed as

$$\begin{aligned}\rho^{\rm I}_{1,2} &= {\rm Tr}_4\left[V_{2,4}\left(|{\rm ECS}\rangle_\tau\langle{\rm ECS}|\otimes|0\rangle_3\langle 0|\right)V^\dagger_{2,4}\right]\\ &= \mathcal{N}^2\Bigg[\left|\frac{\alpha\chi_+}{\sqrt{2}}\right\rangle_1\left\langle\frac{\alpha\chi_+}{\sqrt{2}}\right|\otimes\left|\frac{\beta\chi_+}{\sqrt{2}}\right\rangle_2\left\langle\frac{\beta\chi_+}{\sqrt{2}}\right|\\ &\quad+\left|-\frac{\alpha\chi_-}{\sqrt{2}}\right\rangle_1\left\langle-\frac{\alpha\chi_-}{\sqrt{2}}\right|\otimes\left|\frac{\beta\chi_+}{\sqrt{2}}\right\rangle_2\left\langle\frac{\beta\chi_+}{\sqrt{2}}\right|\\ &\quad+{\rm e}^{(\tau-1)\eta|\alpha|^2}\left|\frac{\alpha\chi_+}{\sqrt{2}}\right\rangle_1\left\langle-\frac{\alpha\chi_-}{\sqrt{2}}\right|\otimes\left|\frac{\beta\chi_-}{\sqrt{2}}\right\rangle_2\left\langle\frac{\beta\chi_+}{\sqrt{2}}\right|\\ &\quad+{\rm e}^{(\tau-1)\eta|\alpha|^2}\left|-\frac{\alpha\chi_-}{\sqrt{2}}\right\rangle_1\left\langle\frac{\alpha\chi_+}{\sqrt{2}}\right|\otimes\left|\frac{\beta\chi_+}{\sqrt{2}}\right\rangle_2\left\langle\frac{\beta\chi_-}{\sqrt{2}}\right|\Bigg].\end{aligned} \tag{30}$$

For simplicity, we define the non-orthogonal basis as

$$\begin{aligned}\left|\Psi^{\rm I}_1\right\rangle &= \left|\frac{\alpha\chi_+}{\sqrt{2}}\right\rangle_1\left|\frac{\beta\chi_-}{\sqrt{2}}\right\rangle_2,\\ \left|\Psi^{\rm I}_2\right\rangle &= \left|-\frac{\alpha\chi_-}{\sqrt{2}}\right\rangle_1\left|\frac{\beta\chi_+}{\sqrt{2}}\right\rangle_2,\end{aligned} \tag{31}$$

which corresponds to Eq. (18) with α and β exchanged. Thus Eq. (30) simplifies to

$$\rho^{\rm I}_{1,2} = \mathcal{N}^2\begin{pmatrix}1 & {\rm e}^{-(1-\tau)\eta|\alpha|^2}\\ {\rm e}^{-(1-\tau)\eta|\alpha|^2} & 1\end{pmatrix}, \tag{32}$$

which closely resembles $\rho^{\rm S}_{1,2}$ in Eq. (19), differing only by the replacement of τ with $1-\tau$. Following the derivation of QFI presented in the previous subsection, we obtain

$$\det\rho^{\rm I}_{1,2} = \mathcal{N}^4\left(1-|p^2|\right)\left(1-{\rm e}^{-2(1-\tau)\eta|\alpha|^2}\right), \tag{33}$$

$$\langle\sigma_3\rangle = 1-2\mathcal{N}^2\left(1-|p|^2\right), \tag{34}$$

$${\rm e}^{{\rm i}\vartheta} = 1, \tag{35}$$

where the overlap between $\left|\Psi^{\rm I}_1\right\rangle$ and $\left|\Psi^{\rm I}_2\right\rangle$ is given by

$$p \equiv \langle\Psi^{\rm I}_1\mid\Psi^{\rm I}_2\rangle = {\rm e}^{-[1-(1-\tau)\eta]|\alpha|^2}. \tag{36}$$

Additionally, we have

$$\left\langle\Psi^{\rm I}_i\right|a^\dagger_1a_1\left|\Psi^{\rm I}_i\right\rangle = \frac{\chi^2_\pm}{2}|\alpha|^2, \tag{37}$$

$$\left\langle\Psi^{\rm I}_i\right|(a^\dagger_1a_1)^2\left|\Psi^{\rm I}_i\right\rangle = \frac{\chi^2_\pm}{2}|\alpha|^2+\frac{\chi^4_\pm}{4}|\alpha|^4, \tag{38}$$

$$\left\langle\Psi^{\rm I}_1\right|a^\dagger_1a_1\left|\Psi^{\rm I}_2\right\rangle = \frac{1-2\tau}{2}|\alpha|^2p, \tag{39}$$

$$\left\langle\Psi^{\rm I}_1\right|(a^\dagger_1a_1)^2\left|\Psi^{\rm I}_2\right\rangle = \frac{1-2\tau}{2}|\alpha|^2p+\frac{(1-2\tau)^2}{4}|\alpha|^4p. \tag{40}$$

It is noteworthy that the expressions in Eqs. (37)–(40) differ from those in Eqs. (24)–(27) by up to a factor of $1-\eta$. Substituting all the above expressions into Eq. (9) yields the QFI.

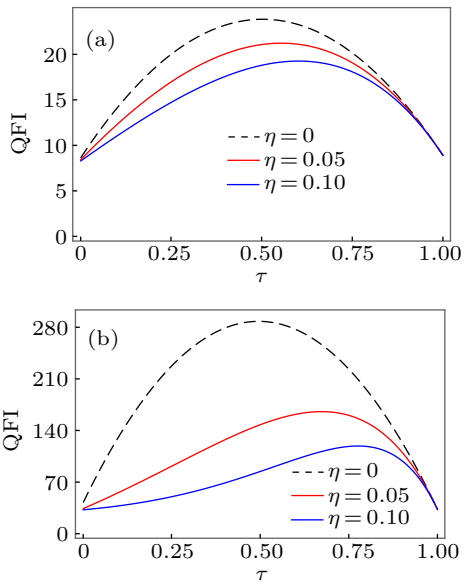


Fig. 4. QFI as a function of the BS transmittance τ. The same plot scheme is used as in Fig. 2.

A similar phenomenon to that observed in the case of photon loss in the signal mode can also be found when photon loss occurs in the idler mode (see Fig. 4). That is an unbalanced BS can enhance phase sensitivity in the presence of single-mode photon loss. However, a notable difference is that as the photon loss becomes stronger, the optimal BS transmittance $\tau_{\rm opt}$ shifts to larger values. This behavior can be explained by the fact that as τ increases, the average photon number in idler mode after the first BS,

$$\langle a^\dagger_2a_2\rangle = \mathcal{N}^2|\alpha|^2\left[1+(2\tau-1)\,{\rm e}^{-|\alpha|^2}\right], \tag{41}$$

increases to compensate for the photon loss in idler mode. Another difference observed in this scenario is that the advantage provided by the unbalanced configuration remains even when the photon loss reaches full strength ($\eta = 1$). This contrasts with the signal-mode photon loss case, where the advantage is eventually lost. These differences are illustrated in Fig. 5.

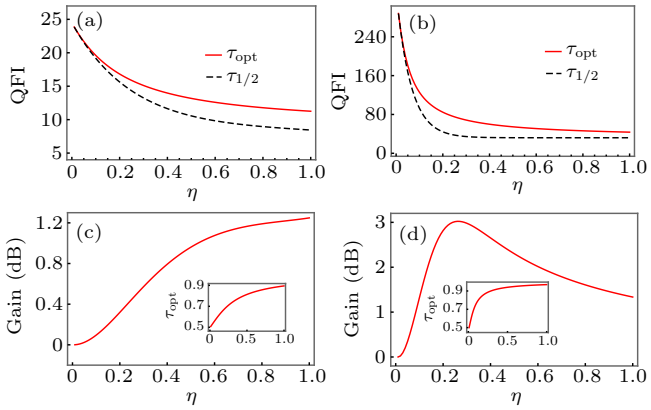


Fig. 5. QFI as a function of the photon loss strength η in the upper panel and the gain defined in Eq. (29) as a function of η in the lower panel. The same plot scheme is used as in Fig. 3.

3.2. Photon loss in two arms

In the following, we consider the case of photon loss occurring in both modes. We assume that the photon loss strength is equal in each mode, as in Refs. [21,25,26]. Following the same procedure as in previous subsections, the density matrix of the system after the photon losses can be derived as

$$\begin{aligned}\rho_{1,2}^{\rm D} &= {\rm Tr}_{3,4}\left[V_{1,3}V_{2,4}\left(|{\rm ECS}\rangle_\tau\langle{\rm ECS}|\otimes|00\rangle_{34}\langle 00|\right)V_{2,4}^\dagger V_{1,3}^\dagger\right]\\ &= \mathcal{N}^2\Bigg[\left|\frac{\beta\chi_+}{\sqrt{2}}\right\rangle_1\left\langle\frac{\beta\chi_+}{\sqrt{2}}\right|\otimes\left|\frac{\beta\chi_-}{\sqrt{2}}\right\rangle_2\left\langle\frac{\beta\chi_-}{\sqrt{2}}\right|\\ &\quad+\left|-\frac{\beta\chi_-}{\sqrt{2}}\right\rangle_1\left\langle-\frac{\beta\chi_-}{\sqrt{2}}\right|\otimes\left|\frac{\beta\chi_+}{\sqrt{2}}\right\rangle_2\left\langle\frac{\beta\chi_+}{\sqrt{2}}\right|\\ &\quad+{\rm e}^{-\eta|\alpha|^2}\left|\frac{\beta\chi_+}{\sqrt{2}}\right\rangle_1\left\langle-\frac{\beta\chi_-}{\sqrt{2}}\right|\otimes\left|\frac{\beta\chi_-}{\sqrt{2}}\right\rangle_2\left\langle\frac{\beta\chi_+}{\sqrt{2}}\right|\\ &\quad+{\rm e}^{-\eta|\alpha|^2}\left|-\frac{\beta\chi_-}{\sqrt{2}}\right\rangle_1\left\langle\frac{\beta\chi_+}{\sqrt{2}}\right|\otimes\left|\frac{\beta\chi_+}{\sqrt{2}}\right\rangle_2\left\langle\frac{\beta\chi_-}{\sqrt{2}}\right|\Bigg].\end{aligned} \tag{42}$$

By defining the non-orthogonal basis

$$\begin{aligned}\left|\Psi_1^{\rm D}\right\rangle &= \left|\frac{\beta\chi_+}{\sqrt{2}}\right\rangle_1\left|\frac{\beta\chi_-}{\sqrt{2}}\right\rangle_2,\\ \left|\Psi_2^{\rm D}\right\rangle &= \left|-\frac{\beta\chi_-}{\sqrt{2}}\right\rangle_1\left|\frac{\beta\chi_+}{\sqrt{2}}\right\rangle_2,\end{aligned} \tag{43}$$

the reduced density matrix from Eq. (42) can be rewritten in the following simplified form:

$$\rho_{1,2}^{\rm D} = \mathcal{N}^2\begin{pmatrix}1 & {\rm e}^{-\eta|\alpha|^2}\\ {\rm e}^{-\eta|\alpha|^2} & 1\end{pmatrix}. \tag{44}$$

We observe that the expressions of Eqs. (43) and (44) are nearly identical to their counterparts in the single-mode photon loss scenario, namely, Eqs. (18) and (19), but with tiny differences: in Eq. (43), both amplitudes in modes 1 and 2 depend on β due to same photon losses in both modes. Additionally, in Eq. (44), the off-orthogonal element does not depend on τ. Due to the similarity to the single-mode photon loss case, the formulae for calculating the QFI given by Eqs. (20)–(27) are also applicable to the double-mode photon loss case. The only differences are that

$$\det\rho_{1,2}^{\rm D} = \mathcal{N}^4\left(1-|p^2|\right)\left(1-{\rm e}^{-2\eta|\alpha|^2}\right), \tag{45}$$

$$p \equiv \langle\Psi_1^{\rm D}\,|\,\Psi_2^{\rm D}\rangle = {\rm e}^{-(1-\eta)|\alpha|^2}, \tag{46}$$

where the exponents in both expressions are independent of τ, unlike in Eqs. (20) and (23).

In Fig. 6 we plot QFI as a function of the BS transmittance τ for the double-mode photon loss scenario. The results show a significantly different behavior from the single-mode photon loss case. Here, the QFI always reaches its maximum at $\tau = 1/2$ and gradually decreases as τ deviates from $1/2$. This suggests that, in the double-mode loss case, a balanced BS is always the optimal configuration, both in lossless and loss scenarios. The decay rate of the QFI decreases as the loss strength η increases. Eventually, when η becomes sufficiently large, the QFI flattens out. This indicates that the QFI becomes almost independent of the parameter τ for large η.

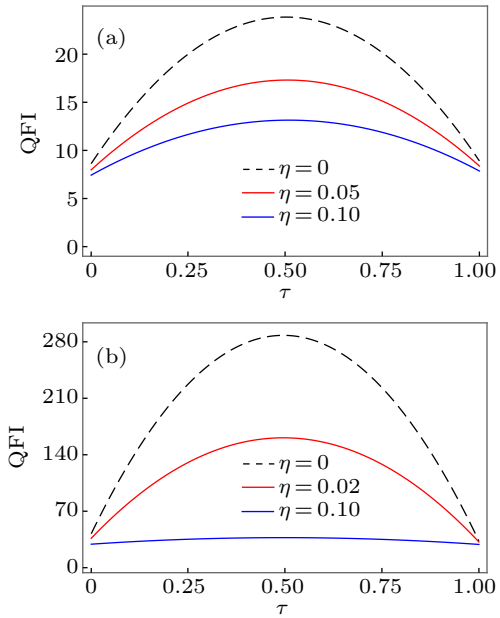


Fig. 6. QFI as a function of the BS transmittance τ. The same plot scheme is used as in Fig. 2.

4. Further discussion

In the previous section, we compared the performance of balanced and unbalanced ECS schemes under single- and double-mode photon loss scenarios for $\alpha < 5$, consistent with the range considered by Joo *et al.*[21] Here, we extend this

analysis to the regime where $\alpha > 5$, corresponding to sufficiently high photon intensities. For this case, we make the following approximations across all previously considered photon loss cases: $\mathcal{N} \approx 1/\sqrt{2}$ and $p \approx 0$, assuming η is moderate. Therefore, all ingredient terms for calculation of the QFI are given by

$$\det \rho^{x}_{1,2} = \begin{cases} \frac{1}{4}\left(1 - \mathrm{e}^{-2\tau\eta|\alpha|^2}\right), & x = \mathrm{S}, \\ \frac{1}{4}\left(1 - \mathrm{e}^{-2(1-\tau)\eta|\alpha|^2}\right), & x = \mathrm{I}, \\ \frac{1}{4}\left(1 - \mathrm{e}^{-2\eta|\alpha|^2}\right), & x = \mathrm{D}, \end{cases} \tag{47}$$

$$\langle \sigma_3 \rangle = 0, \tag{48}$$

$$\mathrm{e}^{\mathrm{i}\vartheta} = 1. \tag{49}$$

For the signal- and double-mode photon loss cases ($x = \mathrm{S}$ and D), the expectations are

$$\langle \Psi_i^x | a_1^\dagger a_1 | \Psi_i^x \rangle = \frac{\chi_\pm^2}{2} |\alpha|^2 (1-\eta), \tag{50}$$

$$\langle \Psi_i^x | (a_1^\dagger a_1)^2 | \Psi_i^x \rangle = \frac{\chi_\pm^2}{2} |\alpha|^2 (1-\eta) + \frac{\chi_\pm^4}{4} |\alpha|^4 (1-\eta)^2. \tag{51}$$

For the idler-mode photon loss case, we get

$$\langle \Psi_i^{\mathrm{I}} | a_1^\dagger a_1 | \Psi_i^{\mathrm{I}} \rangle = \frac{\chi_\pm^2}{2} |\alpha|^2, \tag{52}$$

$$\langle \Psi_i^{\mathrm{I}} | (a_1^\dagger a_1)^2 | \Psi_i^{\mathrm{I}} \rangle = \frac{\chi_\pm^2}{2} |\alpha|^2 + \frac{\chi_\pm^4}{4} |\alpha|^4. \tag{53}$$

These expressions differ from the signal and double-mode photon loss cases by a factor of $1-\eta$. For all three types of photon loss ($x = \mathrm{S}$, I and D), the off-diagonal terms vanish as

$$\langle \Psi_1^x | a_1^\dagger a_1 | \Psi_2^x \rangle = 0, \tag{54}$$

$$\langle \Psi_1^x | (a_1^\dagger a_1)^2 | \Psi_2^x \rangle = 0. \tag{55}$$

Using these results, we obtain the analytical expressions for the QFI for all three types of photon loss

$$F_{\mathrm{S}} = 2|\beta|^2 + 4(1-\tau)\tau \mathrm{e}^{-2\tau\eta|\alpha|^2} |\beta|^4, \tag{56}$$

$$F_{\mathrm{I}} = 2|\alpha|^2 + 4(1-\tau)\tau \mathrm{e}^{-2(1-\tau)\eta|\alpha|^2} |\alpha|^4, \tag{57}$$

$$F_{\mathrm{D}} = 2|\beta|^2 + 4(1-\tau)\tau \mathrm{e}^{-2\eta|\alpha|^2} |\beta|^4, \tag{58}$$

with $\beta = \sqrt{1-\eta}\alpha$. Note that the second term in Eq. (57) reduces to that in Eq. (56) by setting $\tau' \equiv 1-\tau$. In the limit of $\eta \to 0$ (where $\beta \approx \alpha$), the expressions for F_{I} and F_{S} become identical. Due to their similarity, we omit the discussion for F_{I}. Additionally, we note that the difference between the expressions for F_{S} in Eq. (56) and F_{D} Eq. (58) lies in whether the exponent is τ-dependent or τ-independent.

Clearly, in the lossless case ($\eta = 0$), F_x ($x = \mathrm{S}$, I and D) simplify to

$$F_x|_{\eta=0} = 2|\alpha|^2 + 4(1-\tau)\tau|\alpha|^4, \tag{59}$$

which depends on τ. This expression reaches its maximum value of $2|\alpha|^2 + |\alpha|^4$ with $\tau = 1/2$, which is consistent with the result obtained in Ref. [21]. This suggests that in the lossless case the balanced BS is optimal for phase sensitivity.

In the lossy case, according to Eq. (58), for the double-mode photon loss scenario as $\alpha \to \infty$ the QFI reduces to

$$F_{\mathrm{cl}} = 2|\beta|^2, \tag{60}$$

which corresponds to the classical strategy where a coherent state of the amplitude of α is injected into one input port of the interferometer. In contrast, the signal-mode photon loss case behaves quite differently. The presence of the τ-dependent exponent term in Eq. (56) leads to improved sensitivity as $\alpha \to \infty$. To clearly demonstrate this effect, we plot in Fig. 7 the gain in the QFI of Eq. (56) relative to Eq. (60) as

$$g_2 = 10\log_{10}\left(\frac{F_{\mathrm{S}}}{F_{\mathrm{cl}}}\right). \tag{61}$$

From Fig. 7, we see that the gain with the optimal BS transmittance stays high as α increases, while the gain with balanced BS decreases. The insets show that the optimal BS transmittance monotonically decreases with α, approaching but never reaching 0, due to the $\tau(1-\tau)$ term in the second term of Eq. (56). If $\tau = 0$, the sensitivity matches that of the classical strategy.

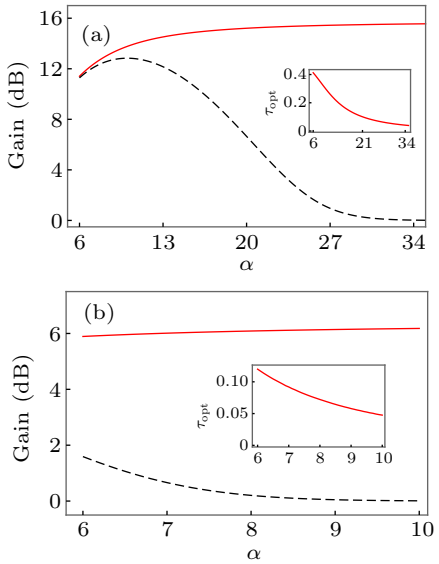


Fig. 7. The gain defined by Eq. (61) as a function of α for $\eta = 0.01$ (a) and $\eta = 0.1$ (b), where photon loss occurs in signal mode. The red solid line represents the gain provided by the unbalanced ECSs with the optimal τ_{opt} and the black dashed line represents that by the balanced ECSs. The optimal BS transmittance τ_{opt} versus α is plotted in the insets.

Here, we note that to achieve a quantum advantage in sensitivity under photon loss, τ must be decreased as α increases. To further illustrate this relationship, a trade-off between α and τ for a given η is plotted in Fig. 8. A closer look at Eq. (56) reveals the reason for this trade-off. The second

term in Eq. (56) primarily contributes to the quantum advantage in sensitivity enhancement. To maintain this advantage, a reasonable way is to adjust τ to be smaller in order to counterbalance the larger α, thereby ensuring that the exponential term $e^{-2\tau\eta|\alpha|^2}$ does not vanish.

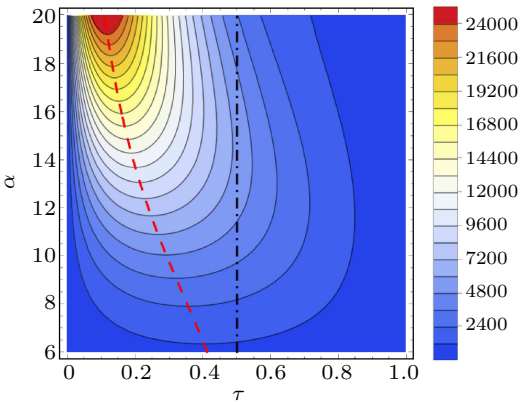


Fig. 8. Contour plot of QFI as a function of α and τ for $\eta = 0.01$. The contour represents the values of QFI for the corresponding parameters. The red dashed line represents the QFI for the optimal BS transmittance $\tau_{\rm opt}$ and the black dot-dashed line represents the QFI for the balanced BS $\tau_{1/2}$.

5. Discussion and conclusion

We have proposed and investigated a quantum-enhanced interferometric scheme using unbalanced ECSs in the presence of both single- and double-mode photon losses. Through a quantitative analysis of the QFI, we have shown that unbalanced ECSs offer superior sensitivity and robustness against photon loss compared with traditional balanced BS configurations under single-mode photon loss. Furthermore, this advantage persists even at high photon intensity, where the balanced configuration becomes metrologically equivalent to the classical strategy using coherent states as input. However, when photon loss occurs equally in both modes, the balanced configuration remains optimal and the ECS scheme provides no advantage over the classical strategy for large photon intensities.

An interferometer with an unbalanced BS has an advantage over a balanced one in phase estimation when photon loss occurs in a single mode. The underlying physics is that adjusting the BS transmission ratio increases photon intensity in the affected arm, thereby compensating for the loss. Other approaches could also be effective, such as using an optical amplifier. However, this method requires active optical elements and is more challenging to implement experimentally than our approach.

Besides, there are many applications that benefit from using an unbalanced BS, such as state truncation,[46] noiseless linear amplification[47] and the creation of hybrid entanglement[48,49] and Schrödinger cat states.[36] Notably, noiseless linear amplification has been widely applied in entanglement distillation[50] and quantum communication,[51,52] and other applications to counteract channel loss.

Appendix A: Derivation of the QFI for an arbitrary two-mode density matrix

In this appendix, we revisit the method for calculating the QFI for an arbitrary two-mode density matrix, following Ref. [25]. Consider a general 2×2 density matrix ρ represented in a non-orthogonal normalized basis $|\Psi_1\rangle$ and $|\Psi_2\rangle$, expressed as

$$\rho = \begin{pmatrix} a & b \\ b^* & c \end{pmatrix}. \tag{A1}$$

To derive the QFI, the key step is to transform the non-orthogonal basis to an orthogonal basis. We first construct a set of new orthogonal basis vectors in $|\Psi_1\rangle$ and $|\Psi_2\rangle$ using the Gram–Schmidt procedure,[53] such that

$$|\Phi_1\rangle = |\Psi_1\rangle, \quad |\Phi_2\rangle = \frac{1}{\sqrt{1-|p|^2}}\left(|\Psi_2\rangle - p\,|\Psi_1\rangle\right), \tag{A2}$$

with $p = \langle\Psi_1 \mid \Psi_2\rangle$ the overlap between $|\Psi_1\rangle$ and $|\Psi_2\rangle$. In the Gram–Schmidt basis $|\Phi_1\rangle$ and $|\Phi_2\rangle$, the density matrix of ρ from Eq. (A1) becomes

$$\rho = \begin{pmatrix} a+bp^*+b^*p+c\,|p|^2 & (b+cp)\sqrt{1-|p|^2} \\ (b^*+cp^*)\sqrt{1-|p|^2} & c\left(1-|p|^2\right) \end{pmatrix}, \tag{A3}$$

satisfying $a+bp^*+b^*p+c\,|p|^2 = 1-c(1-|p|^2)$ due to the normalization condition $\mathrm{Tr}(\rho)=1$. The spectral decomposition of ρ is

$$\rho = \lambda_+ |\lambda_+\rangle\langle\lambda_+| + \lambda_- |\lambda_-\rangle\langle\lambda_-|, \tag{A4}$$

where $\lambda_\pm = \left(1 \pm \sqrt{1-\det\rho}\right)/2$ are the eigenvalues and

$$|\lambda_\pm\rangle = \left(\pm\zeta_\pm e^{i\vartheta},\ \zeta_\mp\right)^{\mathrm{T}} \tag{A5}$$

are the corresponding eigenstates in the Gram–Schmidt basis $|\Phi_1\rangle$ and $|\Phi_2\rangle$. In the above we introduce the following definitions:

$$\zeta_\pm = \sqrt{\frac{\sqrt{1-4\det\rho} \pm \langle\sigma_3\rangle}{2\sqrt{1-4\det\rho}}}, \tag{A6}$$

with

$$\det\rho = \left(1-|p|^2\right)\left(ac-|b|^2\right), \tag{A7}$$

$$\langle\sigma_3\rangle = 1-2c\left(1-|p|^2\right), \tag{A8}$$

$$e^{i\vartheta} = \frac{b+cp}{|b+cp|}. \tag{A9}$$

Hence, the QFI is derived as Eqs. (9)–(11) from Eqs. (4)–(6) by simply replacing p_i and $|\varphi_i\rangle$ $(i=1,2)$ with $\lambda_\pm$ and $|\lambda_\pm\rangle$, respectively. For convenience, the eigenstates of Eq. (A5) in

the orthogonal basis $|\Phi_1\rangle$ and $|\Phi_2\rangle$ can be rewritten in the non-orthogonal basis $|\Psi_1\rangle$ and $|\Psi_2\rangle$ as

$$|\lambda_\pm\rangle = \mathcal{C}_\pm |\Psi_1\rangle + \mathcal{D}_\mp |\Psi_2\rangle, \tag{A10}$$

with

$$\mathcal{C}_\pm = \pm\zeta_\pm e^{i\vartheta} - \frac{p\zeta_\mp}{\sqrt{1-|p|^2}}, \tag{A11}$$

$$\mathcal{D}_\mp = \frac{\zeta_\mp}{\sqrt{1-|p|^2}}. \tag{A12}$$

Acknowledgements

We thank Chun-Mei Zhang for helpful discussions. This work was supported by the National Natural Science Foundation of China (Grant No. 12005106) and the Postgraduate Research and Practice Innovation Program of Jiangsu Province (Grant No. JSCX23-0260). Y. B. S. acknowledges support from the National Natural Science Foundation of China (Grant No. 11974189). L. Z. acknowledges support from the National Natural Science Foundation of China (Grant No. 12175106).

References

[1] Rarity J G, Tapster P R, Jakeman E, Larchuk T, Campos R A, Teich M C and Saleh B E A 1990 *Phys. Rev. Lett.* **65** 1348
[2] Mitchell M W, Lundeen J S and Steinberg A M 2004 *Nature* **429** 161
[3] Walther P, Pan J W, Aspelmeyer M, Ursin R, Gasparoni S and Zeilinger A 2004 *Nature* **429** 158
[4] Wei C Q, Liu J B, Dong Y F, Sun Y N, Zhou Y, Zheng H B, Liu Y Y, Yan X S, Li F L and Xu Z 2024 *Chin. Phys. B* **33** 034203
[5] Liu H L, Wang M J, Bao J X, Liu C, Li Y, Li S J and Wang H 2022 *Chin. Phys. B* **31** 110306
[6] Tse M, *et al.* 2019 *Phys. Rev. Lett.* **123** 231107
[7] Acernese F, *et al.* (Virgo Collaboration) 2019 *Phys. Rev. Lett.* **123** 231108
[8] Gault W and Shepherd G 1982 *Advances in Space Research* **2** 111
[9] Lu T L, Yuan H, Kong L Q, Zhao Y J, Zhang L L and Zhang C L 2016 *Chin. Phys. B* **25** 080702
[10] Wineland D J, Bollinger J J, Itano W M and Heinzen D J1994 *Phys. Rev. A* **50** 67
[11] Leibfried D, Barrett M D, Schaetz T, Britton J, Chiaverini J, Itano W M, Jost J D, Langer C and Wineland D J 2004 *Science* **304** 1476
[12] Afek I, Ambar O and Silberberg Y 2010 *Science* **328** 879
[13] Namkung M, Kim D H, Hong S, Kim Y S, Lee C and Lim H T 2024 *New J. Phys.* **26** 073028
[14] Caves C M 1981 *Phys. Rev. D* **23** 1693
[15] Xiao M, Wu L A and Kimble H J 1987 *Phys. Rev. Lett.* **59** 278
[16] Anisimov P M, Raterman G M, Chiruvelli A, Plick W N, Huver S D, Lee H and Dowling J P 2010 *Phys. Rev. Lett.* **104** 103602
[17] Tan Q S, Liao J Q, Wang X G and Nori F 2014 *Phys. Rev. A* **89** 053822
[18] Carranza R and Gerry C C 2012 *J. Opt. Soc. Am. B* **29** 2581
[19] Wang S, Zhang J and Xu X 2022 *Opt. Commun.* **505** 127592
[20] Xu J H, Wang J Z, Chen A X, Li Y and Jin G R 2019 *Chin. Phys. B* **28** 120303
[21] Joo J, Munro W J and Spiller T P 2011 *Phys. Rev. Lett.* **107** 083601
[22] Chen X T, Zhang R, Lu W J, Zuo Y, Jiao Y F and Kuang L M 2024 *Phys. Rev. A* **109** 042609
[23] Sanders B C 2012 *J. Phys. A: Math. Theor.* **45** 244002
[24] Luis A 2001 *Phys. Rev. A* **64** 054102
[25] Jing X X, Liu J, Zhong W and Wang X G 2014 *Commun. Theor. Phys.* **61** 115
[26] Zhang Y M, Li X W, Yang W and Jin G R2013 *Phys. Rev. A* **88** 043832
[27] Huang W, Liang X, Zhu B, Yan Y, Yuan C H, Zhang W and Chen L Q 2023 *Phys. Rev. Lett.* **130** 073601
[28] Wu S, Zhang D, Li Z, Shi M, Yang P, Guo J, Du W, Bao G and Zhang W 2023 *Phys. Rev. Appl.* **20** 064028
[29] Ataman S 2022 *Phys. Rev. A* **105** 012604
[30] Liu Y J, Wang M Y, Xiang Z C and Wu H B 2022 *Chin. Phys. B* **31** 110305
[31] Helstrom C W 1976 *Quantum Detection and Estimation Theory* (Academic, New York)
[32] Holevo A S 1982 *Probabilistic and Statistical Aspects of Quantum Theory* (North-Holland, Amsterdam)
[33] Braunstein S L and Caves C M 1994 *Phys. Rev. Lett.* **72** 3439
[34] Paris M A T T E O G A 2009 *Int. J. Quantum Inform.* **07** 125
[35] Zhong W, Lu X M, Jing X X and Wang X G 2014 *J. Phys. A: Math. Theor.* **47** 385304
[36] Takase K, Yoshikawa J i, Asavanant W, Endo M and Furusawa A 2021 *Phys. Rev. A* **103** 013710
[37] Wang X, Zhan X, Li Y, Xiao L, Zhu G, Qu D, Lin Q, Yu Y and Xue P 2023 *Phys. Rev. Lett.* **131** 150803
[38] García-Pérez G, Rossi M A, Sokolov B, Tacchino F, Barkoutsos P K, Mazzola G, Tavernelli I and Maniscalco S 2021 *PRX Quantum* **2** 040342
[39] Dorner U, Demkowicz-Dobrzanski R, Smith B J, Lundeen J S, Wasilewski W, Banaszek K and Walmsley I A2009 *Phys. Rev. Lett.* **102** 040403
[40] Demkowicz-Dobrzanski R, Dorner U, Smith B J, Lundeen J S, Wasilewski W, Banaszek K and Walmsley I A 2009 *Phys. Rev. A* **80** 013825
[41] Joo J, Park K, Jeong H, Munro W J, Nemoto K and Spiller T P 2012 *Phys. Rev. A* **86** 043828
[42] Braunstein S L, Caves C M and Milburn G 1996 *Annals of Physics* **247** 135
[43] Ataman S 2020 *Phys. Rev. A* **102** 013704
[44] Bai K, Peng Z, Luo H G and An J H 2019 *Phys. Rev. Lett.* **123** 040402
[45] van Enk S J 2005 *Phys. Rev. A* **72** 022308
[46] Pegg D T, Phillips L S and Barnett S M 1998 *Phys. Rev. Lett.* **81** 1604
[47] Ralph T C and Lund A P 2009 *Proceedings of 9th International Conference*, edited by A. Lvovsky (AIP, New York) pp. 155–160
[48] Wen J, Novikova I, Qian C, Zhang C and Du S 2021 *Photonics* **8**
[49] Jeong H, Zavatta A, Kang M, Lee S W, Costanzo L S, Grandi S, Ralph T C and Bellini M 2014 *Nat. Photon.* **8** 564
[50] Xiang G Y, Ralph T C, Lund A P, Walk N and Pryde G J 2010 *Nat. Photon.* **4** 316
[51] Zhang S, Yang S, Zou X, Shi B and Guo G 2012 *Phys. Rev. A* **86** 034302
[52] Monteiro F, Verbanis E, Vivoli V C, Martin A, Gisin N, Zbinden H and Thew R T 2017 *Quantum Science and Technology* **2** 024008
[53] Nielsen M A and Chuang I L 2000 *Quantum Computation and Quantum Information* (Cambridge: Cambridge University Press)